J|A|C|S COMMUNICATIONS

Published on Web 09/14/2010

Active Site Threonine Facilitates Proton Transfer during Dioxygen Activation at the Diiron Center of Toluene/*o*-Xylene Monooxygenase Hydroxylase

Woon Ju Song,[†] Michael S. McCormick,[†] Rachel K. Behan,[†] Matthew H. Sazinsky,[§] Wei Jiang,[‡] Jeffery Lin,[§] Carsten Krebs,[‡] and Stephen J. Lippard*,[†]

Department of Chemistry, Massachusetts Institute of Technology, Cambridge, Massachusetts 02139, Department of Chemistry, Pomona College, Claremont, California 91711, and Department of Biochemistry and Molecular Biology and Department of Chemistry, The Pennsylvania State University, University Park, Pennsylvania 16802

Received July 19, 2010; E-mail: lippard@mit.edu

Abstract: Toluene/*o*-xylene monooxygenase hydroxylase (ToMOH), a diiron-containing enzyme, can activate dioxygen to oxidize aromatic substrates. To elucidate the role of a strictly conserved T201 residue during dioxygen activation of the enzyme, T201S, T201G, T201C, and T201V variants of ToMOH were prepared by site-directed mutagenesis. X-ray crystal structures of all the variants were obtained. Steady-state activity, regiospecificity, and single-turnover yields were also determined for the T201 mutants. Dioxygen activation by the reduced T201 variants was explored by stopped-flow UV−vis and Mössbauer spectroscopy. These studies demonstrate that the dioxygen activation mechanism is preserved in all T201 variants; however, both the formation and decay kinetics of a peroxodiiron(III) intermediate, $T201_{peroxo}$, were greatly altered, revealing that T201 is critically involved in dioxygen activation. A comparison of the kinetics of O_2 activation in the T201S, T201C, and T201G variants under various reaction conditions revealed that T201 plays a major role in proton transfer, which is required to generate the peroxodiiron(III) intermediate. A mechanism is postulated for dioxygen activation, and possible structures of oxygenated intermediates are discussed.

A role for a strictly conserved threonine residue at the active sites of bacterial multicomponent monooxygenase (BMM) hydroxylases has been discussed for more than a decade.[1−5] In particular, it has been conjectured that the threonine might stabilize a hydrogen-bonding network leading from the protein surface to a metal-bound, active dioxygen moiety, facilitating proton transfer required to generate and stabilize oxygenated intermediates. Such speculation for the function of the threonine residue is based in part on analogy to studies of cytochrome P450 monooxygenase (P450), where a similarly positioned threonine in the distal pocket of the heme site facilitates proton transfer to the distal oxygen atom to form an iron(III) hydroperoxo species, which then converts to an oxoiron(IV) porphyrin π-cation radical.[6−9] Replacing threonine with alanine uncouples this process, liberating hydrogen peroxide. Unlike P450, however, few studies of diiron monooxygenases have been conducted in sufficient detail to determine whether the threonine residue does play a role during O_2 activation and, if so, whether it operates in a manner similar to that of P450. The present Communication addresses these issues.

Toluene/*o*-xylene monooxygenase hydroxylase (ToMOH) is a carboxylate-bridged nonheme-diiron enzyme in the BMM family.[10,11] A threonine residue (T201) is located in the region where dioxygen and hydrocarbons bind adjacent to the diiron active site. Previous structural studies of ToMOH and toluene 4-monooxygenase hydroxylase (T4moH) revealed the hydroxyl group of T201 to be a part of a hydrogen-bonding network within the active site, involving a glutamate ligand (E231), a coordinated water molecule, and, in complex with the regulatory protein (T4moH/T4moD), an ordered water molecule in the cavity.[12,13] In addition, recent studies of a functionally conservative ToMOH variant, T201S, demonstrated that two oxygenated species, $ToMOH_{peroxo}$ and $T201_{peroxo}$ (previously designated as $T201S_{peroxo}$ in ref 14), were generated upon reaction of the reduced hydroxylase ($ToMOH_{red}$) and regulatory protein (ToMOD) with O_2. The latter intermediate exhibits an optical band at ∼600−800 nm ($\varepsilon_{675\,nm} \approx 1500\ cm^{-1}\ M^{-1}$).[14] The visible spectrum of $T201_{peroxo}$ allowed us to measure the formation and decay kinetics of the oxygenated species. The ability to probe the formation mechanism of $T201_{peroxo}$ from O_2 provides insight into the oxygenation chemistry of ToMOH, which is particularly useful because kinetic studies of the native enzyme are hampered by the lack of a UV−vis optical transition for $ToMOH_{peroxo}$.

Here we report the results of our studies of the T201 variants, T201C, T201G, and T201V, prepared by site-directed mutagenesis, which elucidate the effects of the T201 side chain in regulating the kinetics of the $T201_{peroxo}$ and reveal its function during O_2 activation. We also report the X-ray crystal structures, steady-state activities, regiospecificity for toluene and *o*-xylene oxidation, and single-turnover yields of the T201 variants.

X-ray crystal structure determinations of all four T201 variants revealed the absence of any global structural differences or dramatic

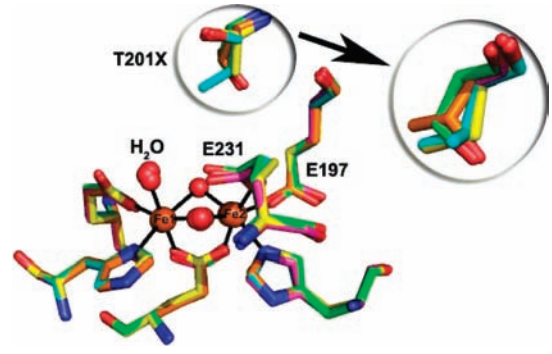

Figure 1. Overlaid X-ray crystal structures of ToMOH wild-type (PDB 2INC, orange) and T201X variants: T201S (green), T201G (pink), T201C (yellow), and T201V (cyan). Iron atoms and water/hydroxide ligands are represented as orange and red spheres, respectively. Ligands and T201X residues are depicted as sticks. Nitrogen and oxygen atoms are colored in blue and red, respectively. T201X residues are rotated counter-clockwise and expanded for clarity.

[†] Massachusetts Institute of Technology.
[§] Pomona College.
[‡] The Pennsylvania State University.

10.1021/ja1063795

Table 1. Steady-State Activity and Single-Turnover Yield of T201X ToMOH Variants

	WT	T201S	T201G	T201C	T201V
specific activity (mU/mg)	1100 ± 100	2400 ± 300	1900 ± 200	1600 ± 200	390 ± 20
k_{cat} (s^{-1})	0.04 ± 0.01	0.08 ± 0.04	0.08 ± 0.02	0.09 ± 0.02	0.016 ± 0.009
k_{cat}/K_M ($s^{-1}\mu M^{-1}$)	0.02 ± 0.01	0.017 ± 0.009	$(2.0 \pm 0.9) \times 10^{-4}$	$(2.8 \pm 0.8) \times 10^{-4}$	$(1.3 \pm 0.9) \times 10^{-4}$
single-turnover yield (%)	56 ± 7	59 ± 6	33 ± 8	26 ± 1	27 ± 9

shift in the geometry of the T201 backbone or side-chain atoms (Figure 1 and Supporting Information Table S1 and Figure S1). The overlaid structures of wild-type and T201 variants indicate that the diiron(III) cofactors and coordinating ligands are well aligned. The orientation of the hydroxyl group in T201S is identical to that of the wild-type enzyme, suggesting that the T201S variant retains the capacity to form hydrogen-bonding interactions in the active site similar to those in the native protein. In contrast, the hydrophobic side chains of T201G, T201C, and T201V do not participate in hydrogen bonding. One notable feature is rotation about the $C_\alpha - C_\beta$ bond in both the T201C and T201V variants, where thiol and methyl groups, respectively, point in the same direction as the methyl group of the wild-type enzyme toward the hydrophobic cavity.

The steady-state activity of the T201 variants was measured using phenol as the substrate (Table 1). The maximum product formation rates, calculated as the specific activity, are comparable for all T201 variants, ranging from 0.3 to 2.2 times the wild-type activity. Michaelis−Menten kinetics of the T201 variants were also determined (Table 1 and Supporting Information Figure S2). The catalytic rate constants (k_{cat}) for all T201 variants are similar to those of the wild type, indicating that substitution of the T201 side chain does not significantly perturb the maximum efficiency for aromatic hydroxylation. In contrast, substrate specificity, as revealed by the k_{cat}/K_M values, is diminished by about 2 orders of magnitude in the T201G, T201C, and T201V variants. This result suggests that the lack of a hydroxyl group at the T201 position in these variants perturbs at least one step during catalysis. A similar effect was observed for toluene 4-monooxygenase hydroxylase (T4moH)[5] and for P450[6−9] when the analogous threonine residues were replaced with alanine residues.

The regiospecificity for phenol oxidation in the T201 variants does not change, producing exclusively 2-hydroxyphenol. For toluene oxidation, however, the T201C, T201V, and T201G variants exhibit significant changes in product distribution (Supporting Information Table S2). These results indicate that the T201 substitutions reshape the substrate-binding pocket, altering the orientation of substrate in the active site. The T201 variants also gave different product distributions for *o*-xylene oxidation. The ratio of the two products, 2,3-dimethylphenol and 3,4-dimethylphenol, reflects the steric environment at the T201 sites, with the bulkier side chains conveying a higher ratio of 3,4-dimethylphenol vs 2,3-dimethylphenol. This finding suggests that the side chain of the T201 residue may guide and orient hydrocarbon substrates as they enter the diiron active site. It is plausible that the side chain of the T201 residue also interacts with dioxygen during catalysis.

To further characterize the O_2 activation reaction in T201 variants of ToMOH and understand which chemical step in this process is perturbed by the T201 substitution, a premixed solution of $ToMOH_{red}$ T201 variants and ToMOD ($ToMOH_{red}D$) was treated with O_2-saturated buffer and monitored by freeze-quench Mössbauer and stopped-flow UV−vis spectroscopy. Two of the variants, T201G and T201C, also exhibit broad, transient optical features that absorb maximally at ~675 nm (Supporting Information Figure S3), which are identical to those observed for the T201S variant.[14] The Mössbauer spectrum of a sample of the T201G $ToMOH_{red}D$, which was allowed to react for 15 s with O_2, the time of maximum accumulation of the 675 nm feature observed by stopped-flow UV−vis spectrophotometry, reveals the presence of ~10% of a quadrupole doublet with parameters nearly identical to those reported for $T201_{peroxo}$ in T201S ToMOH (Supporting Information Figure S4).[14] In addition, the spectrum reveals the presence of other diiron(III) species, which amount to 35 ± 7% of the total intensity of the spectrum.

Table 2. Formation and Decay Rate Constants of $T201_{peroxo}$ in the Reaction of T201X $ToMOH_{red}$:D with Dioxygen[a]

	k_{form} (s^{-1})	k_{decay} (s^{-1})
T201S	130 ± 7[b]	2.9 ± 0.2
T201C	93 ± 3	1.9 ± 0.2, 0.23 ± 0.03
T201G	0.11 ± 0.01	0.035 ± 0.003
T201V	n.d.[c]	n.d.[c]

[a] The reaction was observed by stopped-flow spectrophotometry in 25 mM MOPS pH 7.0 buffer at 4 °C. [b] This value for the formation rate constant differs slightly from the previously reported 85 ± 11 s^{-1} because it varies between batches of purified protein. [c] Not determined.

The kinetics of $T201_{peroxo}$ formation and decay in the T201C/G/S variants were investigated by monitoring the absorption at 675 nm over time and fitting the traces on the basis of the model described below (Table 2 and Supporting Information Figure S5). The formation and decay rates of $T201_{peroxo}$ in the T201C variant were best fit to three consecutive, irreversible reactions, consisting of one formation and two consecutive decay processes ascribed to $ToMOH_{red} \rightarrow T201_{peroxo} \rightarrow T201^*_{peroxo} \rightarrow ToMOH_{ox}$, where $T201^*_{peroxo}$ and $ToMOH_{ox}$ are the sequential decay products of $T201_{peroxo}$. Alternatively, the biphasic decay in T201C may be the result of two (or more) decay pathways of $T201_{peroxo}$. The reaction kinetics for $T201_{peroxo}$ in the T201G variant were similarly measured. The A_{675}-vs-time trace is biphasic and was fit to a model involving two irreversible reactions corresponding to $ToMOH_{red} \rightarrow T201_{peroxo} \rightarrow ToMOH_{ox}$. The formation rate constant of $T201_{peroxo}$ in T201C is nearly identical to that of the T201S variant. The formation rate constant in the T201G variant, however, is ~700 times lower than that in the T201S variant. The similarity in formation kinetics of $T201_{peroxo}$ in T201S and T201C implies that the thiol group of T201C may function like a hydroxyl group, at least during formation of $T201_{peroxo}$, whereas the lack of a functional group in the T201G variant dramatically reduces the rate of $T201_{peroxo}$ formation. The striking difference in $T201_{peroxo}$ formation kinetics in the T201 variants indicates that the rate-determining step for $T201_{peroxo}$ formation can be greatly perturbed and that the T201 residue is critically involved in controlling the kinetics of dioxygen activation.

Although the formation and decay of $T201_{peroxo}$ could be studied for the T201S and T201C variants, no optical bands appeared in the UV−vis region upon the addition of O_2 to the T201V $ToMOH_{red}$ protein. This result indicates that the lack of a hydrogen-bonding residue in the T201 position retards a key chemical step involved in formation of $T201_{peroxo}$, presumably proton transfer. At present we cannot rule out the possibility that $T201_{peroxo}$ is not generated in the T201V enzymes due to the changes in the thermodynamic stability of the various oxygenated species.[15] For T201G, which forms a $T201_{peroxo}$ intermediate, a solvent-derived proton may serve

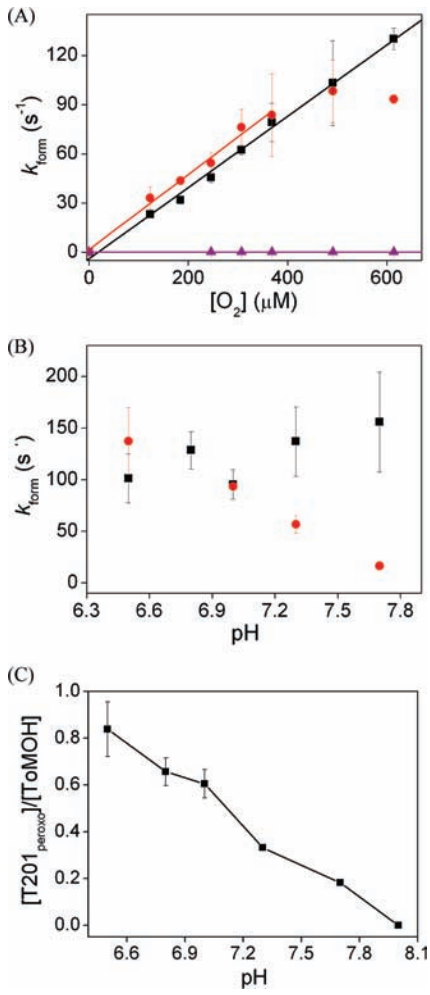

Figure 2. Formation rates and the concentration of $T201_{peroxo}$ in T201 variants. (A) Formation rates measured in the reaction of various dioxygen concentrations with T201S (black squares), T201C (red circles), and T201G (purple triangles). (B) Formation rates of $T201_{peroxo}$ in the T201S (black squares) and T201C (red circles) under various pH values. (C) The ratio of $T201_{peroxo}$ to total protein concentration formed in the reaction of T201S with O_2 under various pH values.

as the hydrogen-bonding residue. There is presumably room for such in the active site of T201G but not in the T201V variant.

To elucidate the mechanism of $T201_{peroxo}$ formation and the role of the T201 residue in this process, kinetic studies were performed at variable temperature, variable O_2 and H^+ concentrations, and with D_2O as solvent. When the dioxygen concentration was varied in its reaction with T201S $ToMOH_{red}D$, the formation rate constants (k_{form}) were linearly proportional to [O_2], yielding a second-order rate constant of $k_2 = 0.22 \pm 0.01\ s^{-1}\ \mu M^{-1}$ (Figure 2A, black squares). The results demonstrate that $T201_{peroxo}$ is generated in an irreversible process and that formation of $T201_{peroxo}$ is kinetically limited by the bimolecular reaction between $ToMOH_{red}$ and O_2. From these data, k_{form} of $T201_{peroxo}$ in T201S enzyme can be represented as k[O_2] ($k_{form} = k$[O_2]). To our knowledge, this behavior reveals the first example where dioxygen has been determined to be rate-limiting in a pre-steady-state reaction of any BMM hydroxylase enzyme. This interpretation is strongly supported by the negative value of $\Delta S^{\ddagger}$, -71 ± 2 J mol^{-1} K^{-1} (Supporting Information Figure S6). We therefore conclude that chemical steps during O_2 activation, such as structural rearrangements in the active site, component interactions, and water/proton translocation, occur much more rapidly than the associative reaction with dioxygen.

The rate constants for $T201_{peroxo}$ formation at various pH values (Figure 2B, black squares) and in D_2O were also measured. From pH 6.5 to 7.7, the formation rate constant does not change significantly. When the buffer was prepared with deuterium oxide (pL = 7.0 at 5 °C), the kinetic solvent isotope effect (KSIE) was 0.92 ± 0.11, consistent with our hypothesis that proton translocation is not kinetically involved in this process.

Proton transfer is, however, indispensable to the formation of $T201_{peroxo}$. By fitting the time-resolved optical spectra to the model $ToMOH_{red} \rightarrow T201_{peroxo} \rightarrow ToMOH_{ox}$ using the measured molar absorptivity of $T201_{peroxo}$ from the UV−vis and Mössbauer data, we can estimate the concentration of $T201_{peroxo}$ generated from the reaction of $ToMOH_{red}$ with dioxygen and the fraction of $T201_{peroxo}$ formed compared to total protein (Figure 2C). When the ratio was measured under various pH conditions, more $T201_{peroxo}$ was generated at higher proton concentrations, indicating that proton transfer is coupled to dioxygen consumption, although it is not observed kinetically.

In the T201C variant, the $T201_{peroxo}$ formation rate constants vary linearly with [O_2] over the range ∼150−400 μM. At higher O_2 concentrations, however, a plateau is reached (Figure 2A, red circles). The partial O_2-dependence for $T201_{peroxo}$ formation in the T201C enzyme indicates that the rate is not simply limited by the dioxygen diffusion to the active site ($k_{form} \neq k$[O_2]). Reactions not involved in the rate-determining step for the T201S variant are slowed solely due to the T201S → T201C mutation. The $T201_{peroxo}$ formation rate constants for the T201C enzyme display nonlinear Eyring behavior over the 4−16 °C temperature range. This nonlinearity could arise from a temperature-dependent combination of multiple processes involved in $T201_{peroxo}$ formation in T201C, rather than a simple associative reaction between the hydroxylase and O_2 (Figure S6). The formation rate constant depends on pH, indicating that higher proton concentrations accelerate the formation of $T201_{peroxo}$ (Figure 2B, red circles). These results reveal that the rate-determining step of $T201_{peroxo}$ formation in the T201C variant changes from that in the T201S variant to reflect a combination of O_2 associative and proton-transfer events.

The T201G mutation evoked an even more substantial effect on the $T201_{peroxo}$ formation kinetics. The rate constants displayed no dependence on O_2 concentration over an ∼150−612 μM range (Figure 2A, purple triangles), and the $\Delta S^{\ddagger}$ value of -35 ± 3 J mol^{-1} K^{-1} for $T201_{peroxo}$ formation is significantly less negative as a result of the T201S → T201G mutation (Figure S6). These data indicate that formation of $T201_{peroxo}$ in ToMOH T201G is also controlled by a different chemical step than occurs in the T201S enzyme (see above). The KSIE value for the formation process in T201G is 5.7 ± 0.7, indicating generation of $T201_{peroxo}$ to be limited by a requisite proton translocation step. The large KSIE value observed for the T201G enzyme implies that one or more proton translocation steps are involved in the rate-determining step of $T201_{peroxo}$ formation,[16] possibly involving the shifting carboxylate (E231, vide infra). Proton-assisted dissociation of the E231 bridging oxygen atom may accompany O_2 binding and activation at the diiron center.

These studies demonstrate that several chemical steps representing $T201_{peroxo}$ formation are altered by substitution of T201 in ToMOH. We can assume that an associative reaction of dioxygen at the diiron center (k[O_2]) occurs for all T201 variants. In T201S, this step is rate-limiting because proton transfer is rapid. In T201C and T201G, proton transfer is the slow step and is followed by more rapid O_2 binding. Removal of the hydroxyl group at the T201 position disturbs the formation kinetics of $T201_{peroxo}$ by retarding proton transfer ($k_{form} \approx k$[H^+]). These data definitively support the long-standing hypothesis that a hydroxyl group at residue T201

Scheme 1. Proposed Mechanism of Dioxygen Activation in T201 Variants of ToMOH[a]

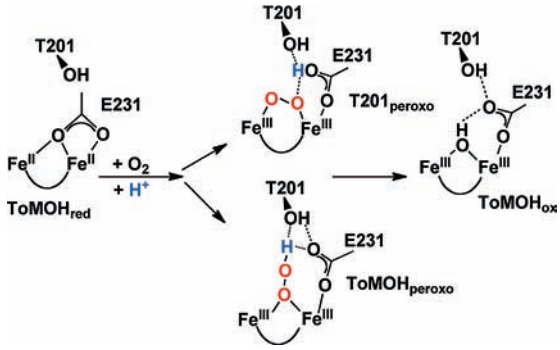

[a] The oxygen atoms originating from dioxygen are colored in red; the incoming proton is colored blue. Possible hydrogen bonds between T201, E231, and oxygenated intermediates are represented as dotted lines. A water molecule might be positioned between the side chains of residues T201 and E231.

plays a major role in the facilitation of proton transfer during O_2 activation in ToMO and most likely all BMMs.

On the basis of these pre-steady-state kinetics of $T201_{peroxo}$ in T201 variants, we propose a chemical mechanism for dioxygen activation, Scheme 1. Consumption of dioxygen is coupled to the proton transfer into the active site, followed by formation of $T201_{peroxo}$. The protonation of the peroxo unit in $T201_{peroxo}$, however, is unlikely because it would quench the peroxo-to-iron charge-transfer optical bands.[17] Instead, we postulate that the proton is transferred to the adjacent and shifting glutamate residue (E231), a process was recently demonstrated in a synthetic diiron model complex.[18] This proton could then form a hydrogen bond to the adjacent oxygen atom in the $T201_{peroxo}$, possibly a μ-1,2-peroxo-diiron(III) unit.[19−21] In contrast, the proton transfer directly to the peroxo moiety can lead to the formation of $ToMOH_{peroxo}$, which exhibits no optical bands. A μ-1,1-hydroperoxodiiron(III) unit is proposed as the structure of $ToMOH_{peroxo}$ on the basis of QM/MM, DFT, and Mössbauer computational studies.[15]

The decay rate of $T201_{peroxo}$ is also significantly altered in the T201 variants (Table 2). The decay rates decrease in the same order as the formation rates. Since the primary decay pathway of $ToMOH_{peroxo}$ in the absence of hydrocarbon substrates is protonation of the peroxo unit and subsequent release of hydrogen peroxide,[22] the decay rates of the T201 variants may be also related to their abilities to facilitate proton transfer. Further studies to clarify this process are in progress.

In conclusion, steady-state activity, single-turnover yields, and pre-steady-state kinetics studies of the dioxgyen activation by T201 variants of ToMOH support the long-standing but previously untested hypothesis that the hydroxyl group in T201 plays a major role in catalysis. The kinetics of $T201_{peroxo}$ formation in T201 variants under pre-steady-state conditions demonstrate that this threonine residue controls formation and decay rates of $T201_{peroxo}$ by facilitating proton translocation during dioxygen activation. The role of T201 in ToMOH that we have uncovered here is analogous to that of threonine near the active site of P450,[6−8] supporting a general threonine-dependent process as Nature's strategy to control proton transfer. The proposed mechanism of dioxygen activation explains how a minor change in the proton-transfer pathway can lead to the formation of discrete oxygenated intermediates, $ToMOH_{peroxo}$ and $T201_{peroxo}$, in toluene monooxygenases.

Acknowledgment. This work was supported by grant GM32134 (to S.J.L.) from the National Institute of General Medical Sciences and by a grant from Research Corporation (to M.H.S). R.K.B. acknowledges fellowship support from the NIGMS (1 F32 GM084564-02). We thank C. E. Tinberg for comments on the manuscript. Crystallographic coordinates have been deposited in the RCSB databank, with accession codes 3N1X, 3N1Y, 3N1Z, and 3N20, for T201C, T201G, T201S, and T201V, respectively.

Supporting Information Available: Detailed experimental methods; table of X-ray data collection parameters, phase determination, and refinement statistics for the structures; table of product distribution in toluene and *o*-xylene oxidation; and figures showing active sites, Michaelis−Menten kinetics, time-dependent Mössbauer and UV−vis spectral changes upon reaction with dioxygen, and kinetics of $T201_{peroxo}$ under various conditions in T201 variants. This material is available free of charge via the Internet at http://pubs.acs.org.

References

(1) Rosenzweig, A. C.; Frederick, C. A.; Lippard, S. J.; Nordlund, P. *Nature* **1993**, *366*, 537–543.
(2) Lee, S.-K.; Lipscomb, J. D. *Biochemistry* **1999**, *38*, 4423–4432.
(3) Pikus, J. D.; Mitchell, K. H.; Studts, J. M.; McClay, K.; Steffan, R. J.; Fox, B. G. *Biochemistry* **2000**, *39*, 791–799.
(4) Lovell, T.; Li, J.; Noodleman, L. *Inorg. Chem.* **2001**, *40*, 5267–5278.
(5) Elsen, N. L.; Bailey, L. J.; Hauser, A. D.; Fox, B. G. *Biochemistry* **2009**, *48*, 3838–3846.
(6) Imai, M.; Shimada, H.; Watanabe, Y.; Matsushima-Hibiya, Y.; Makino, R.; Koga, H.; Horiuchi, T.; Ishimura, Y. *Proc. Natl. Acad. Sci. U.S.A.* **1989**, *86*, 7823–7827.
(7) Martinis, S. A.; Atkins, W. M.; Stayton, P. S.; Sligar, S. G. *J. Am. Chem. Soc.* **1989**, *111*, 9252–9253.
(8) Yeom, H.; Sligar, S. G.; Li, H.; Poulos, T. L.; Fulco, A. J. *Biochemistry* **1995**, *34*, 14733–14740.
(9) Altarsha, M.; Benighaus, T.; Kumar, D.; Thiel, W. *J. Am. Chem. Soc.* **2009**, *131*, 4755–4763.
(10) Sazinsky, M. H.; Lippard, S. J. *Acc. Chem. Res.* **2006**, *39*, 558–566.
(11) Murray, L. J.; Lippard, S. J. *Acc. Chem. Res.* **2007**, *40*, 466–474.
(12) Sazinsky, M. H.; Bard, J.; Di Donato, A.; Lippard, S. J. *J. Biol. Chem.* **2004**, *279*, 30600–30610.
(13) Bailey, L. J.; McCoy, J. G.; Phillips, G. N., Jr.; Fox, B. G. *Proc. Natl. Acad. Sci. U.S.A.* **2008**, *105*, 19194–19198.
(14) Song, W. J.; Behan, R. K.; Naik, S. G.; Huynh, B. H.; Lippard, S. J. *J. Am. Chem. Soc.* **2009**, *131*, 6074–6075.
(15) Bochevarov, A. D.; Li, J.; Song, W. J.; Lippard, S. J.; Friesner, R. A. Manuscript in preparation, 2010.
(16) Vidakovic, M.; Sligar, S. G.; Li, H.; Poulos, T. L. *Biochemistry* **1998**, *37*, 9211–9219.
(17) Jensen, K. P.; Bell, C. B.; Clay, M. D.; Solomon, E. I. *J. Am. Chem. Soc.* **2009**, *131*, 12155–12171.
(18) Do, L. H.; Hayashi, T.; Moënne-Loccoz, P.; Lippard, S. J. *J. Am. Chem. Soc.* **2010**, *132*, 1273–1275.
(19) Kim, K.; Lippard, S. J. *J. Am. Chem. Soc.* **1996**, *118*, 4914–4915.
(20) Moënne-Loccoz, P.; Baldwin, J.; Ley, B. A.; Loehr, T. M.; Bollinger, J. M., Jr. *Biochemistry* **1998**, *37*, 14659–14663.
(21) Skulan, A. J.; Brunold, T. C.; Baldwin, J.; Saleh, L.; Bollinger, J. M., Jr.; Solomon, E. I. *J. Am. Chem. Soc.* **2004**, *126*, 8842–8855.
(22) Murray, L. J.; Naik, S. G.; Ortillo, D. O.; García-Serres, R.; Lee, J. K.; Huynh, B. H.; Lippard, S. J. *J. Am. Chem. Soc.* **2007**, *129*, 14500–14510.

JA1063795